Enhancing omnidirectional mobile robot trajectory tracking robustness using super-twisting observer-based sliding mode control

Dinh Anh Nguyen[1], Viet Phuong Pham[1] and Manh Linh Nguyen[1,*]

[1]*Hanoi University of Science and Technology*
[*]*Corresponding author E-mail: linh.nguyenmanh@hust.edu.vn*
DOI: https://doi.org/10.64032/mca.v30i2.401

Abstract

Four-wheeled Mecanum mobile robots have been increasingly adopted in various modern applications, especially in complex or confined environments, owing to their ability to achieve omnidirectional motion without changing body orientation. However, the nonlinear nature of their dynamics, together with external disturbances during operation, necessitates a robust control strategy. This paper proposes a practical approach that integrates a sliding mode controller to ensure stable trajectory tracking and a super-twisting sliding mode observer to enhance system robustness while mitigating the chattering effect typically associated with sliding mode control. The effectiveness of the proposed scheme is validated through numerical simulations, which demonstrate improved tracking performance and strong resilience to disturbances.

Keywords: *Mobile robot; Sliding controler; Supertwisting sliding mode observer; Trajectory tracking control; Robust control.*

1. Introduction

Recently, with the growing demand for Industry 4.0 technologies, omnidirectional mobile robots have attracted considerable attention and are widely applied across various fields of society. Thanks to their superior maneuverability compared to traditional mobile robots, omnidirectional robots can move easily and flexibly in constrained spaces. The mobility of omnidirectional robots is particularly useful in the design of various service robots, such as smart electric wheelchairs, healthcare robots, mobile manipulation robots, and more. As a result, omnidirectional mobile robots have been extensively researched by scientists in recent years [1–7].

Among various wheel types used in omnidirectional mobile robots, the Mecanum wheel has proven to be one of the most effective solutions for achieving full omnidirectional mobility. A Mecanum wheel can be regarded as a conventional wheel equipped with multiple passive rollers mounted around its circumference. These rollers are typically oriented at a 45^0 angle with respect to the wheel's rotational axis, generating lateral forces that enable motion in any direction. The most common and practical configuration employs four independently driven Mecanum wheels [8–13]. This four-wheel arrangement offers several advantages, including true omnidirectional movement and the ability to maintain continuous operation even under a single-actuator fault condition. However, this also leads to a more complex motion control problem due to its nonlinear nature, and other uncertainties such as friction, model deviations [14–18].

To address the aforementioned control challenges, a wide range of control strategies has been proposed, including classical feedback control, feedback schemes incorporating disturbance observers, and model-free control (MFC) [19–24]. For highly nonlinear systems such as the four-Mecanum-wheeled mobile robot (4-MWMR), one of the most commonly adopted approaches is robust control, particularly sliding mode control (SMC). SMC offers notable advantages, including a straightforward design procedure and strong robustness against system uncertainties. However, its practical implementation is often hindered by the chattering phenomenon in the control signal, which can adversely affect the actuators [16–19],[25]. Another potential approach is the MFC, which eliminates the need for an accurate dynamic model of the 4-MWMR and thus reduces reliance on parameter identification. Nevertheless, MFC methods depend heavily on a lumped disturbance observer, making parameter tuning challenging and potentially limiting performance. Intelligent control techniques, such as fuzzy control and adaptive control, have also been explored in recent studies on mobile robot motion control [23–27]. For example, in [26], a backstepping fuzzy sliding mode controller was proposed to address trajectory tracking in the presence of disturbances. In contrast, an adaptive super-twisting sliding mode controller was developed in [20, 28] to enhance system robustness. Although these approaches offer improved performance, their algorithmic complexity leads to considerable computational burden, which may negatively impact real-time implementation and increase system cost.

Since the super-twisting extended state observer (STESO) was first introduced by Li et al. in 2022 [29], its application to nonlinear systems such as ground mobile robots has attracted increasing attention. For instance, STESO has recently been employed in the control of a ballbot system, demonstrating its effectiveness in disturbance estimation and robustness enhancement [30]. Nevertheless, to the best of the authors' knowledge,

Received: 4 December 2025; Revised: 28 January 2026; Accepted: 9 March 2026.

the application of the STESO to 4-MWMRs has not yet been reported in the literature. In this research, for the first time, the integration of a super-twisting extended state observer into the control system of a 4-MWMR is conducted. In details, a sliding mode controller (SMC) with a proportional–integral–derivative (PID) sliding surface is employed to ensure the stability of the path-following control system first. Then, an STESO is developed to compensate for modeling uncertainties and resistive forces arising from static and viscous friction. By incorporating the STESO, the chattering effect typically associated with SMC is significantly reduced, thereby enhancing the overall performance of the controlled system while maintaining a low computational burden. The effectiveness of the proposed control scheme is evaluated through numerical simulations.

2. Mathematical model of 4-MWMR

2.1 Kinematic model of the 4-MWMR

A Mecanum wheel is essentially a traditional wheel with a series of passive rollers mounted around its circumference. These rollers typically have their axles angled at 45^o relative to the wheel's rotation axis, as shown in Fig 1. Due to this unique structure, the FMWMP (Four-Motor Wheeled Mobile Platform) has an additional degree of freedom compared to conventional differential-drive robots, meaning the FMWMP can move in any direction without needing to change the robot's orientation. Mecanum wheels are divided into two types: $+45^o$ mecanum wheels and -45^o mecanum wheels [9–13].

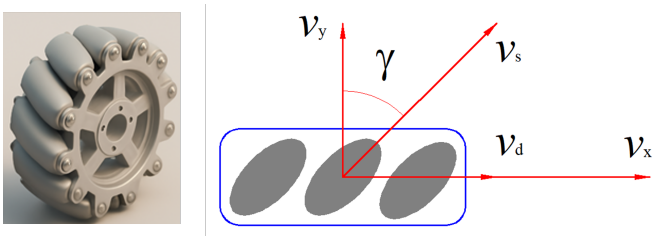

Figure 1: Mecanum Wheel

During the motion of the Mecanum wheel on a surface, with an angular velocity around the wheel axis $\dot{\theta}$, the roller's tilt angle $\gamma = -45^o$, and the wheel diameter R, the absolute velocity of the wheel v can be decomposed into components v_x, v_y, v_s, v_d as shown in Fig. 1. In this case, we have:

$$\dot{\theta}R = v_x - v_y \tan\gamma \tag{1}$$

Substituting $\gamma = -45^o$ into (1), it gives:

$$\dot{\theta} = \frac{1}{R}\begin{bmatrix}1 & -1\end{bmatrix}\begin{bmatrix}v_x \\ v_y\end{bmatrix} \tag{2}$$

Similarly, substituting $\gamma = +45^o$ into (1), it also results in:

$$\dot{\theta} = \frac{1}{R}\begin{bmatrix}1 & 1\end{bmatrix}\begin{bmatrix}v_x \\ v_y\end{bmatrix} \tag{3}$$

When the mobile robot is configured with four Mecanum wheels as shown in Fig 2, the following conditions are met: $\gamma_1 = \gamma_3 = 45^o$, $\gamma_2 = \gamma_4 = -45^o$. Additionally, the direction and orientation of the velocities of each wheels are as in Fig 2. With $(\dot{x}_r, \dot{y}_r, \omega_z)$ representing the vehicle's velocity along the X,

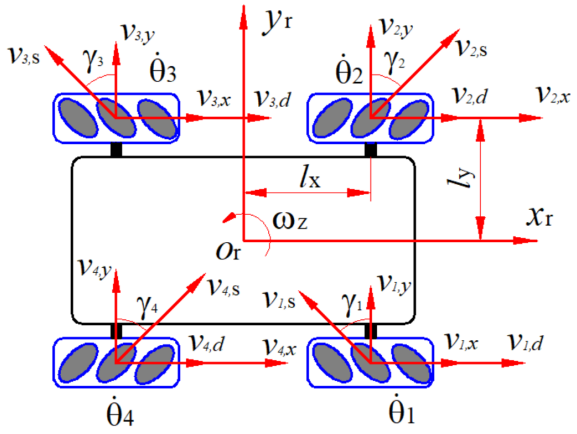

Figure 2: The orientation of the velocity at each wheel

Y and Z axes. Then, the relationship between the velocity at each wheel and the vehicle's body velocity can be established as follows:

$$\dot{\theta}_1 = \frac{1}{R}\begin{bmatrix}1 & 1 & l_x + l_y\end{bmatrix}\begin{bmatrix}\dot{x}_r \\ \dot{y}_r \\ \omega_z\end{bmatrix} \tag{4}$$

$$\dot{\theta}_2 = \frac{1}{R}\begin{bmatrix}1 & -1 & -l_x - l_y\end{bmatrix}\begin{bmatrix}\dot{x}_r \\ \dot{y}_r \\ \omega_z\end{bmatrix} \tag{5}$$

$$\dot{\theta}_3 = \frac{1}{R}\begin{bmatrix}1 & 1 & -l_x - l_y\end{bmatrix}\begin{bmatrix}\dot{x}_r \\ \dot{y}_r \\ \omega_z\end{bmatrix} \tag{6}$$

$$\dot{\theta}_4 = \frac{1}{R}\begin{bmatrix}1 & -1 & l_x + l_y\end{bmatrix}\begin{bmatrix}\dot{x}_r \\ \dot{y}_r \\ \omega_z\end{bmatrix} \tag{7}$$

From (4), (5), (6), and (7), the kinematic model of the 4-MWMR with respect to its body's reference frame is [9–15]:

$$\begin{bmatrix}\dot{\theta}_1 \\ \dot{\theta}_2 \\ \dot{\theta}_3 \\ \dot{\theta}_4\end{bmatrix} = \frac{J}{R}\begin{bmatrix}\dot{x}_r \\ \dot{y}_r \\ \omega_z\end{bmatrix} \tag{8}$$

In which, J is the Jacobian matrix and is expressed by

$$J = \begin{bmatrix}1 & 1 & l_x + l_y \\ 1 & -1 & -l_x - l_y \\ 1 & 1 & -l_x - l_y \\ 1 & -1 & l_x + l_y\end{bmatrix} \tag{9}$$

When the robot's body reference frame is introduced into the global reference frame as in Fig 3, the relationship between the origin coordinates and the robot's body coordinates can be established by:

$$\begin{bmatrix}\dot{x}_q \\ \dot{y}_q \\ \dot{\phi}\end{bmatrix} = \Re(\phi)\begin{bmatrix}\dot{x}_r \\ \dot{y}_r \\ \omega_z\end{bmatrix} \tag{10}$$

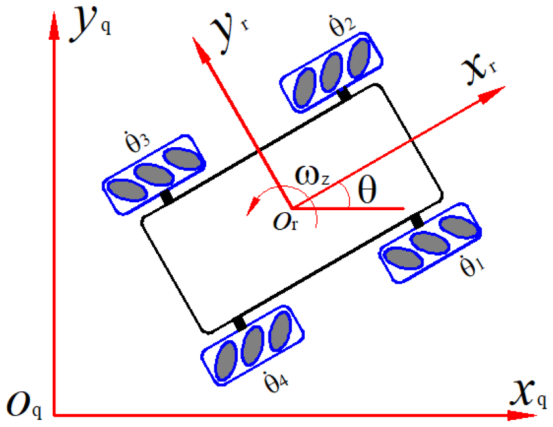

Figure 3: The relationship between the origin coordinates and the robot's body coordinates

Where the transformation matrix $\Re(\phi)$ is expressed by:

$$R(\phi) = \begin{bmatrix} cos(\phi) & -sin(\phi) & 0 \\ sin(\phi) & cos(\phi) & 0 \\ 0 & 0 & 1 \end{bmatrix} \tag{11}$$

2.2 Dynamics model of the 4-MWMR

In constructing the robot's dynamic model, the Euler-Lagrange is applied as follows [6–8]:

$$K = \frac{1}{2}m(\dot{x}_r^2 + \dot{y}_r^2) + \frac{1}{2}J_z\omega_z^2 + \frac{1}{2}J_\omega(\dot{\theta}_1^2 + \dot{\theta}_2^2 + \dot{\theta}_3^2 + \dot{\theta}_4^2) \tag{12}$$

Where m is the robot's mass; J_z is the moment of inertia of the robot about the z axis; J_ω is the wheel's moment of inertia about its own rotation axis. Additionally, the dissipated energy can be defined by:

$$D = \frac{1}{2}D_\theta(\dot{\theta}_1^2 + \dot{\theta}_2^2 + \dot{\theta}_3^2 + \dot{\theta}_4^2) \tag{13}$$

Where D_θ is the friction coefficient.

Consider the Lagrangian function: $L = K - V$, where V is the potential energy of the robot. Since the robot moves only on a flat surface, $V = 0$. Applying the Euler–Lagrange equation, the FMWMR's dynamic model can be defined as follows:

$$\frac{\partial}{\partial t}\frac{\partial}{\partial \dot{\theta}}L - \frac{\partial}{\partial \theta}L = \tau - (\frac{\partial}{\partial \dot{\theta}}D + F(\dot{\theta})) \tag{14}$$

In which,
$\tau = \begin{bmatrix} \tau_1 & \tau_2 & \tau_3 & \tau_4 \end{bmatrix}^T$ is the torque generated by motors.
$F = \begin{bmatrix} f_1 sgn(\dot{\theta}_1) & f_2 sgn(\dot{\theta}_2) & f_3 sgn(\dot{\theta}_3) & f_4 sgn(\dot{\theta}_4) \end{bmatrix}^T$ is the static friction force acting on the robot's wheels.
$\dot{\theta} = \begin{bmatrix} \dot{\theta}_1 & \dot{\theta}_2 & \dot{\theta}_3 & \dot{\theta}_4 \end{bmatrix}^T$ is the angular velocity of the robot's wheels.
From (8), (13), and (14), dynamic model of the 4-MWMR is:

$$\tau = M\ddot{\theta} + D_\theta\dot{\theta} + F \tag{15}$$

With,

$$M = \begin{bmatrix} C & -B & B & D \\ -B & C & D & B \\ B & D & C & -B \\ D & B & -B & C \end{bmatrix}$$

$$A = \frac{mR^2}{8}; B = \frac{J_z R^2}{16(l_x + l_y)^2}; C = A + B + J_\omega; D = A - B;$$

Since the modeling error and external disturbance always exist in practice, (15) is rewritten in a practical forms as follows:

$$\tau + \tau_d = (M + \Delta M)\ddot{\theta} + (D_\theta + \Delta D_\theta)\dot{\theta} + F \tag{16}$$

Where τ_d, ΔM, and ΔD_θ represent unknown disturbances. The simplification of (16) is:

$$\tau + \tau_d + H_d = M\ddot{\theta} + D_\theta\dot{\theta} + F \tag{17}$$

Where $H_d = -\Delta M\ddot{\theta} - \Delta D_\theta\dot{\theta}$ and $\tau_d + H_d$ are referred to as the generalized disturbances in the system.

To conduct the control design, (17) is converted into a state-space model through the following steps. First, define the state variable Z_1 and Z_2 as:

$$\begin{aligned} Z_1 &= \begin{bmatrix} x_q & y_q & \phi_q \end{bmatrix}^T \\ Z_2 &= \begin{bmatrix} \dot{x}_q & \dot{y}_q & \dot{\phi}_q \end{bmatrix}^T \end{aligned} \tag{18}$$

Then, a fundamental manipulation on (8), (10), and (17) yields

$$\begin{cases} \dot{Z}_1 = Z_2 \\ \dot{Z}_2 = -f_z + R\zeta^+ M^{-1}\tau + H \end{cases} \tag{19}$$

In which,

$$\begin{aligned} \zeta^+ &= (\zeta^T\zeta)^{-1}\zeta^T \\ f_z &= (\zeta^+\dot{\zeta} + D_\theta\zeta^+ M^{-1}\zeta)Z_2 + R\zeta^+ M^{-1}F \\ H &= R\zeta^+ M^{-1}[H_d + \tau_d] \end{aligned} \tag{20}$$

$$\begin{aligned} \zeta = JR^{-1}(\phi) &= \begin{bmatrix} \sqrt{2}\cos(\phi_a) & \sqrt{2}\sin(\phi_a) & (l_x + l_y) \\ \sqrt{2}\sin(\phi_a) & -\sqrt{2}\cos(\phi_a) & -(l_x + l_y) \\ \sqrt{2}\cos(\phi_a) & \sqrt{2}\sin(\phi_a) & -(l_x + l_y) \\ \sqrt{2}\sin(\phi_a) & -\sqrt{2}\cos(\phi_a) & (l_x + l_y) \end{bmatrix} \\ \phi_a &= \phi + \pi/4 \\ \dot{\zeta} &= \dot{\phi}\begin{bmatrix} -\sqrt{2}\sin(\phi_a) & \sqrt{2}\cos(\phi_a) & 0 \\ \sqrt{2}\cos(\phi_a) & \sqrt{2}\sin(\phi_a) & 0 \\ -\sqrt{2}\sin(\phi_a) & \sqrt{2}\cos(\phi_a) & 0 \\ \sqrt{2}\cos(\phi_a) & \sqrt{2}\sin(\phi_a) & 0 \end{bmatrix} \end{aligned} \tag{21}$$

Finally, the nonlinear state-space of the 4-MWMR is

$$\begin{cases} \dot{Z}_1 = Z_2 \\ \dot{Z}_2 = -A_z Z_2 + B_z u + Z_3 \end{cases} \tag{22}$$

With,

$$\begin{aligned} A_z &= \zeta^+\dot{\zeta} \\ B_z &= R\zeta^+ M^{-1} \\ Z_3 &= R\zeta^+ M^{-1}(H_d + \tau_d) - D_\theta\zeta^+ M^{-1}\zeta Z_2 \\ u &= \begin{bmatrix} \tau_1, \tau_2, \tau_3, \tau_4 \end{bmatrix}^T \end{aligned} \tag{23}$$

It should be noted from (22) and (23) that all unknown terms—including modeling errors, external disturbances, and system friction (i.e., viscous, static, and rolling friction)—are collectively distinguished and represented by the state variable Z_3. This arrangement allows the subsequent control design to be formulated more clearly and systematically.

3. Control design

3.1 SMC with PID sliding surface

The control strategy offered in this study is shown in Fig. 4, which consists of an SMC with a PID sliding surface, and an STESO that play a very important role in enhancing the robustness of the controlled system while minimising the chattering phenomenon [31–35].

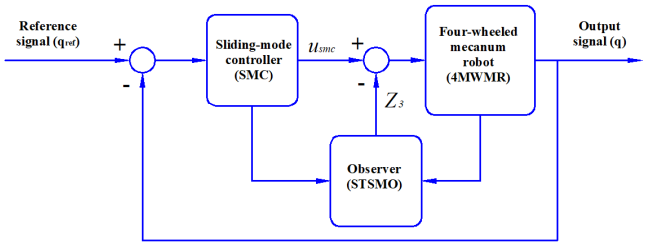

Figure 4: Structure of the Sliding-Mode Controller for a Robot

To carry out the control design, define the sliding variable as:

$$S = 2\zeta\omega_n e(t) + \frac{de(t)}{dt} + \omega_n^2 \int e(t)d(t) \tag{24}$$

In which $\zeta = \frac{1}{\sqrt{2}}$ is the optimal damping factor, ω_n is the bandwidth of the tracking error's dynamics, and the tracking error is:

$$e(t) = Z_{1,ref} - Z_1 \tag{25}$$

Differentiate both sides of (24) gives:

$$\dot{S} = \ddot{e}(t) + 2\zeta\omega_n\dot{e}(t) + \omega_n^2 e(t) \tag{26}$$

It can be deduced from (22) and (25) that

$$\begin{aligned} \dot{e}(t) &= Z_{2,ref} - Z_2 \\ \ddot{e}(t) &= \dot{Z}_{2,ref} - \dot{Z}_2 \end{aligned} \tag{27}$$

Then, by substituting (27) into (26), it results in

$$\dot{S} = \dot{Z}_{2,ref} + 2\zeta\omega_n\dot{e}(t) + \omega_n^2 e(t) + A_z Z_2 - B_z u - Z_3 \tag{28}$$

Now, the equivalent control signal of the SMC can be obtained by neglecting the unknown term Z_3, and solving the following equation

$$\dot{S} = 0 \tag{29}$$

which results in

$$u_{eq} = \frac{1}{R} M\zeta \left(\dot{Z}_{2,ref} + 2\zeta\omega_n\dot{e} + \omega_n^2 e + A_z Z_2\right) \tag{30}$$

To stabilise the controlled system in the presence of the disturbance Z_3, an additional nonlinear control signal u_{sw} is introduced:

$$u_{sw} = \frac{1}{R} M\zeta K_{sw} sign(S) \tag{31}$$

With an assumption that the disturbance Z_3 is bounded, i.e., $||Z_3|| < \Gamma$, and the gain K_{sw} fulfills

$$K_{sw} > \Gamma \tag{32}$$

Then, the final control action of the SMC, which guarantees that the tracking error approaches zero asymptotically, is

$$u_{smc} = \frac{1}{R} M\zeta \left[\dot{Z}_{2,ref} + 2\zeta\omega_n\dot{e} + \omega_n^2 e + A_z Z_2 + K_{sw} sign(S)\right] \tag{33}$$

The stability of the controlled system (22) with control action (33) can be proved by selecting the following Lyapunov candidate function V

$$V = \frac{1}{2} S^T S \tag{34}$$

Differentiate both sides of (34) gives

$$\dot{V} = S^T \dot{S} \tag{35}$$

From (28), (33) and (35), it can be derived that

$$\dot{V} = S^T \left[-Z_3 - K_{sw} sign(S)\right] \tag{36}$$

By taking the assumption (32) in to account, it can be realised that $\dot{V} < 0$, which means the stability of the controlled system is guaranteed.

3.2 STESO design

It is evident from (36) that the system's stability is predominantly governed by the switching gain K_{sw} associated with the nonlinear control signal (31). However, this gain is also the major contributor to the chattering phenomenon. To solve this problem, an STESO is designed to estimate the unknown disturbance Z_3 as follows [27–29].

Consider the following extended dynamic model of the 4-MWMR:

$$\begin{cases} \dot{Z}_1 = Z_2 \\ \dot{Z}_2 = -A_z Z_2 + B_z u + Z_3 \\ \dot{Z}_3 = f \end{cases} \tag{37}$$

With an assumption that f is bounded, i.e.,

$$||f|| < \gamma \tag{38}$$

The STESO is designed as

$$\begin{cases} \dot{\hat{Z}}_1 = \hat{Z}_2 + \beta e_1 \\ \dot{\hat{Z}}_2 = -A_z \hat{Z}_2 + B_z u + \hat{Z}_3 + U_a \\ \dot{\hat{Z}}_3 = k_3 sign(\delta) + k_4 \delta \end{cases} \tag{39}$$

In which β is a positive number, U_a is an auxiliary control variable that needs to be appropriately designed, δ is the sliding variable of the STESO, expressed by

$$\delta = ce_1 + e_2 \tag{40}$$

with $c > 0$, and the estimation errors e_1, e_2 are

$$\begin{cases} e_1 = Z_1 - \hat{Z}_1 \\ e_2 = Z_2 - \hat{Z}_2 \end{cases} \tag{41}$$

By taking the difference of expressions (37) and (39), the dynamic of the estimation error is

$$\begin{cases} \dot{e}_1 = e_2 - \beta e_1 \\ \dot{e}_2 = -A_z e_2 + e_3 - Ua \\ \dot{e}_3 = f - k_3 sign(\delta) - k_4 \delta \end{cases} \tag{42}$$

Now, differentiate both sides of (40) and take (42) into account, it gives

$$\dot{\delta} = \left[cI - A_z\right] e_2 - c\beta e_1 + e_3 + U_a \tag{43}$$

Then, by choosing the auxiliary control signal U_a as:

$$U_a = \left[cI - A_z\right] e_2 - c\beta e_1 + k_1 |\delta|^{\frac{1}{2}} sign(\delta) + k_2 \delta \tag{44}$$

Consequently, the STESO dynamic is obtained and expressed by:

$$\begin{cases} \dot{\delta} & = e_3 - k_1 |\delta|^{\frac{1}{2}} sign(\delta) - k_2 \delta \\ \dot{e}_3 & = f - k_3 sign(\delta) - k_4 \delta \end{cases} \tag{45}$$

With the auxiliary control signal (44), the sliding variable δ converges to the origin in finite time, and the estimation errors converge to zero asymptotically [29].

With $\hat{Z}_3$ estimated from (39), equation (33) can now be reformulated as follows

$$u_{smc} = \frac{1}{R} M \zeta \left[\dot{Z}_{2,ref} + 2\zeta\omega_n \dot{e} + \omega_n^2 e + A_z Z_2 + K_\varepsilon sign(S) - \hat{Z}_3\right] \tag{46}$$

Now, substitute (46) into (36), a simple manipulation gives

$$\dot{V} = S^T \left[\hat{Z}_3 - Z_3 - K_\varepsilon sign(S)\right] \tag{47}$$

Once the stability of the dynamical system (45) is guaranteed, the estimation error $\hat{Z}_3 - Z_3$ is bounded by a very small positive number ε, i.e., $||\hat{Z}_3 - Z_3|| < \varepsilon$. And it is evident that $||\hat{Z}_3 - Z_3|| \ll ||Z_3||$, or in other words, $\varepsilon \ll \Gamma$. As a result, the stability of the controlled system (22) with control signal (46) can be guaranteed by choosing K_ε that fulfills

$$\varepsilon < K_\varepsilon \ll \Gamma \tag{48}$$

Inequality (48) also indicates that the chattering effect of the SMC, when combined with the STESO, is significantly attenuated, which is particularly beneficial for practical implementations.

4. Simulations and discussion

In this section, numerical simulations in various scenarios are conducted to verify the effectiveness of the proposed control strategy. Nominal parameters of the 4-MWMR are provided in Table 1, while the parameters of the SMC and the STESO are as in Table 2, respectively. To fairly evaluate the merit of the proposed strategy over the conventional SMC, a unique circular trajectory described by (49) is employed. Furthermore, the control designed is conducted with the nominal model only, while all simulations are carried out under realistic conditions, i.e., with the existence of the payload described by (50), and external disturbance at time instance $t = 15s$.

$$\begin{cases} x_{ref} = sin(0.2t) \\ y_{ref} = cos(0.2t) \\ \phi_{ref} = sin(0.2t) \end{cases} \tag{49}$$

$$\begin{cases} \Delta m = 20(kg) \\ \Delta J_z = J_z * 0.5(kgm^2) \\ \Delta J_\omega = J_\omega * 0.5(kgm^2) \end{cases} \tag{50}$$

Table 1: Robot simulation parameters

Parameter	Value	Unit
Mass (m)	40	kg
Width of two wheels (l_x)	0.6	m
Length of two wheels (l_y)	0.6	m
Wheel radius (R)	0.076	m
Moment of inertia J_z	4.1	kg·m^2
Moment of inertia J_ω	0.029	kg·m^2
Viscous friction coefficient K_v	0.005	–
Rolling friction coefficient K_r	0.084	–
Static friction coefficient K_s	0.54	–

Table 2: SMC parameters

Parameter	Value	Unit
Bandwidth (ω_0)	4π	–
Switching gain (k_{sw})	4	–
Damping factor (ζ)	0.9	–

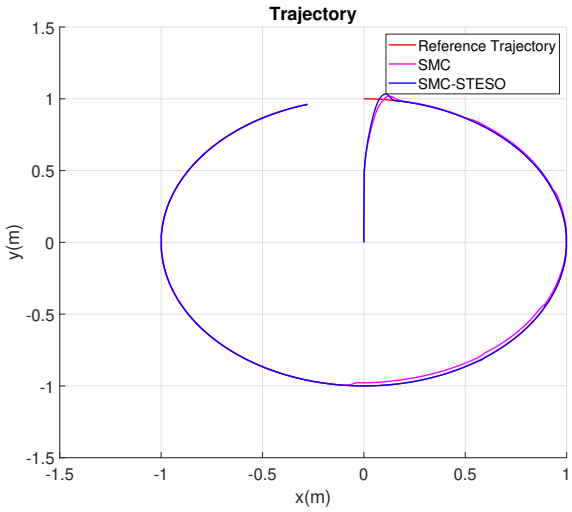

Figure 5: Comparative trajectory tracking performance: SMC vs SMC-STESO

In the first scenario, simulations with the conventional SMC and the SMC-STESO are conducted. Main comparative simulation results, including the trajectory, the sliding variable, the torques command, and the tracking error, are shown in Fig. 5, Fig. 6, Fig. 7, and Fig. 8, respectively. As can be realized, the overall performance of the conventional is poor, mainly due to the chattering as seen in Fig. 6 and Fig. 7, despite the torques are restricted in a reasonable range, i.e., $-15Nm < T < 15Nm$ which is assumed to be the limitation of the motors used in this research. In contrast, the SMC-STESO shows much better performance in terms of chattering-free, as well as accuracy, thanks to the excellent performance of the STESO since it quickly estimate the disturbance as illustrated in Fig. 9

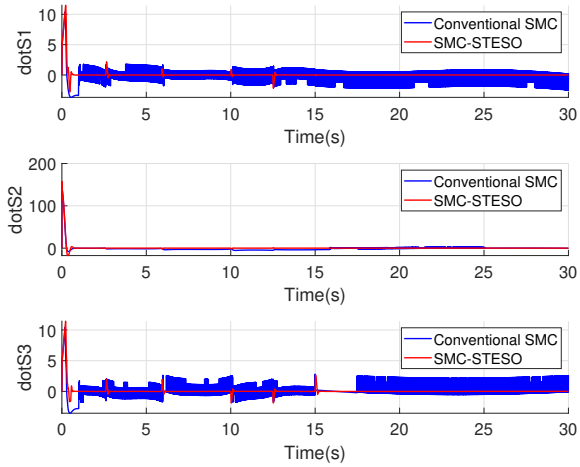

Figure 6: Comparative sliding variables: SMC vs SMC-STESO

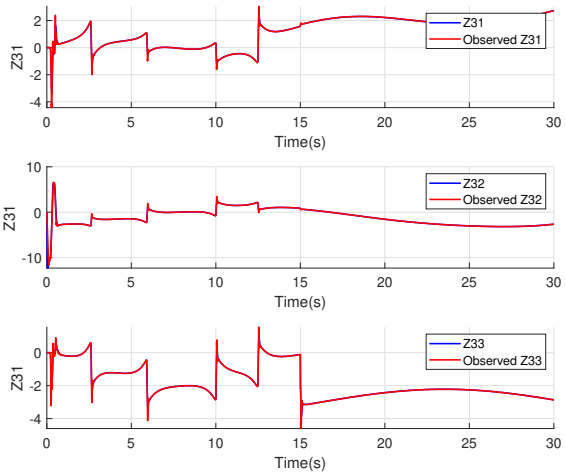

Figure 9: STESO performance

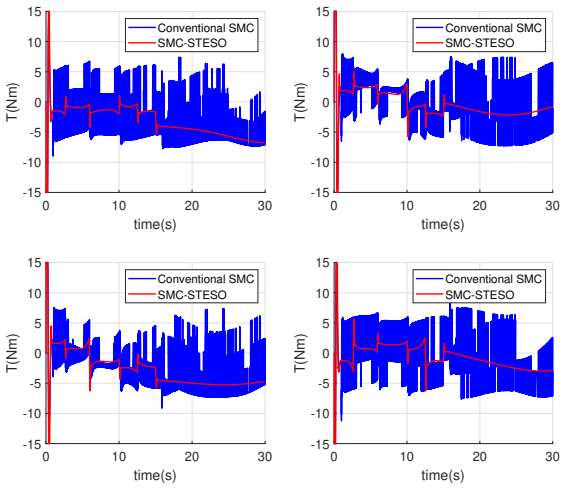

Figure 7: Torque command: SMC vs SMC-STESO

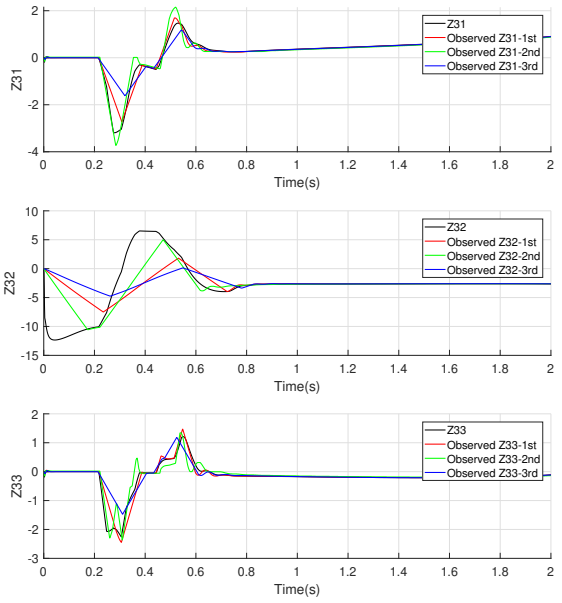

Figure 10: Influence of parameters on performance of the STESO

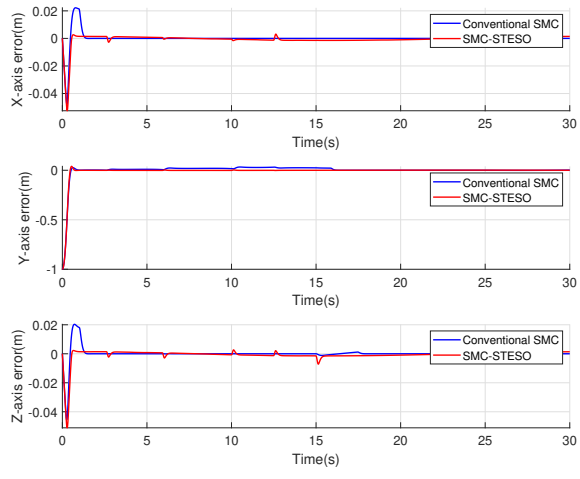

Figure 8: Comparative tracking errors: SMC vs SMC-STESO

Table 3: STESO parameters

Parameter	Value	Unit
β	10	–
c	50	–
Case 1		
$k_1 = k_3$	30	–
$k_2 = k_4$	50	–
Case 2		
$k_1 = k_3$	60	–
$k_2 = k_4$	100	–
Case 3		
$k_1 = k_3$	15	–
$k_2 = k_4$	25	–

As can be observed, the STESO plays a crucial role in de-

termining the overall performance of the SMC–STESO scheme. Therefore, proper tuning of the STESO parameters is of significant importance. Figure 10 illustrates the STESO responses obtained with different gain values listed in Table 3. It can be seen that the steady-state performance remains nearly unchanged, whereas the transient behavior is strongly parameter-dependent. Specifically, higher gain values result in a faster convergence rate but induce larger fluctuations. Based on this observed trend, the tuning of the STESO parameters can be performed with reduced effort.

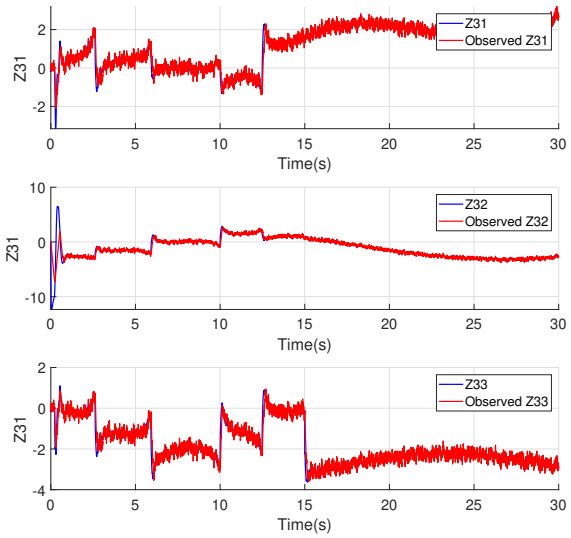

Figure 11: STESO performance under the influence of measurement noise

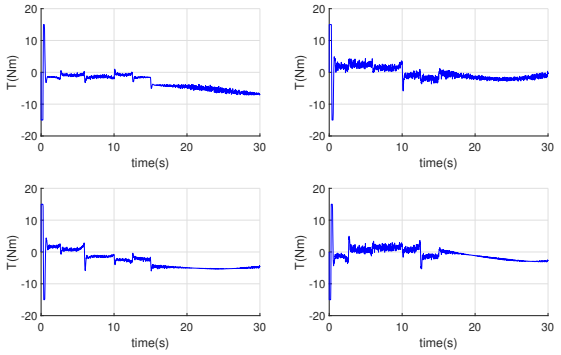

Figure 12: Torque command under the influence of measurement noise

The feasibility of the SMC-STESO is verified by conducting a simulation in the worst case, where significant measurement noise is taken into account. Main results are provided in Fig. 11 to Fig. 12. Figure 9 shows that the STESO remains effective in tracking the disturbance despite a slight degradation in performance, which leads to the appearance of high-frequency torque ripple. However, this slight degradation does not significantly affect the ability of the mobile robot to track its reference path as seen in Fig. 13, thanks to the large inertia of the 4-MWMR, which can effectively absorbs the high-frequency torque ripple.

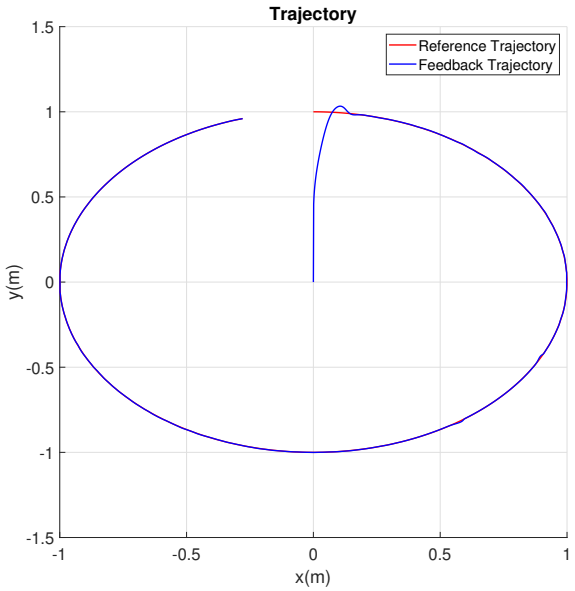

Figure 13: Trajectory tracking performance under the influence of measurement noise

Finally, the integral of absolute error (IAE) criterion, defined in (51) is employed to quantitatively evaluate the performance of the proposed control strategy. As shown in Fig. 14, the overall IAE values obtained with the SMC–STESO scheme are consistently lower than those of the conventional SMC. More specifically, the presence of measurement noise—which inevitably exists in practical applications—has only a marginal impact on the control performance. These results demonstrate the effectiveness and practical feasibility of the proposed SMC–STESO strategy.

$$IAE = \int_0^T |e(t)|\,dt \tag{51}$$

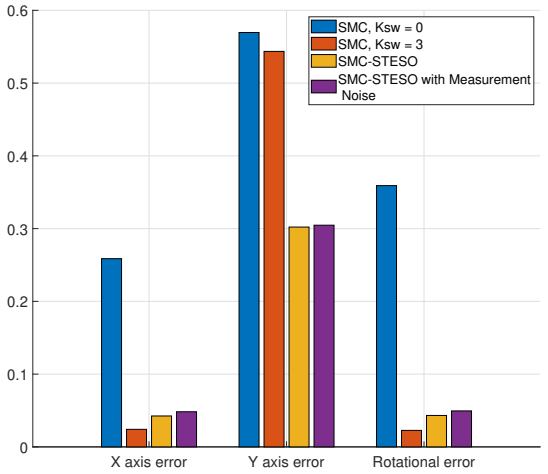

Figure 14: Comparative integral of error between methods

5. Conclusion

In this study, for the first time, the STESO is successfully integrated into the control framework of a 4-MWMR.

First, the nonlinear dynamics of the 4-MWMR are reformulated into a state-space representation, in which unknown and unreliable components—including modeling uncertainties induced by payload variations and resistive forces arising from static and viscous friction—are explicitly separated and lumped into an extended state variable. Subsequently, the STESO is employed to rapidly and accurately estimate this extended variable. By exploiting the estimated disturbance information, the nonlinear switching control action responsible for chattering in conventional SMC is effectively eliminated. As a result, the proposed SMC–STESO strategy achieves chattering-free operation while preserving robustness. Numerical simulation results demonstrate that the SMC–STESO scheme provides superior trajectory tracking performance compared with the conventional SMC in terms of accuracy and chattering suppression, even under significant measurement noise. Moreover, the proposed SMC–STESO approach is well-suited for real-time embedded implementation, as it does not require solving an optimization problem at each sampling instant, unlike model predictive control or adaptive control methods.

References

[1] O.O. Martins et al. “Wheeled Mobile Robot Path Planning and Path Tracking Controller Algorithms: A Review”. In: *Journal of Engineering Science and Technology Review* 13 (June 2020), pp. 152–164. DOI: 10.25103/jestr.133.17.

[2] Andreas Mueller. “Modern Robotics: Mechanics, Planning, and Control [Bookshelf]”. In: *IEEE Control Systems Magazine* 39.6 (2019), pp. 100–102. DOI: 10.1109/MCS.2019.2937265.

[3] Jovina Seau Ling Leong, Kenneth Tze Kin Teo, and Hou Pin Yoong. “Four Wheeled Mobile Robots: A Review”. In: *2022 IEEE International Conference on Artificial Intelligence in Engineering and Technology (IICAIET)*. 2022, pp. 1–6. DOI: 10.1109/IICAIET55139.2022.9936855.

[4] Guoxing Bai et al. “Review and Comparison of Path Tracking Based on Model Predictive Control”. In: *Electronics* 8.10 (2019). ISSN: 2079-9292. DOI: 10.3390/electronics8101077.

[5] Mahmoud El-Sayyah, Mohamad R. Saad, and Maarouf Saad. “Nonlinear Model Predictive Control for Trajectory Tracking of Omnidirectional Robot Using Resilient Propagation”. In: *IEEE Access* 13 (2025), pp. 112642–112653. DOI: 10.1109/ACCESS.2025.3583596.

[6] Tevfik Yiğit. “Modelling and control of the PEMFC powered wheeled mobile robot”. In: *International Journal of Hydrogen Energy* 143 (July 2025), pp. 1154–1162. DOI: 10.1016/j.ijhydene.2025.01.097.

[7] Tian Zhang and Xiangyin Zhang. “Distributed Model Predictive Control with Particle Swarm Optimizer for Collision-Free Trajectory Tracking of MWMR Formation”. In: *Actuators* 12.3 (2023). ISSN: 2076-0825. DOI: 10.3390/act12030127.

[8] Zhenyi Yuan et al. “Trajectory tracking control of a four mecanum wheeled mobile platform: an extended state observer-based sliding mode approach”. In: *IET Control Theory & Applications* 14.3 (2020), pp. 415–426. DOI: https://doi.org/10.1049/iet-cta.2018.6127.

[9] Chunqiao He et al. “Analysis of the Mecanum wheel arrangement of an omnidirectional vehicle”. In: *Proceedings of the Institution of Mechanical Engineers, Part C: Journal of Mechanical Engineering Science* 233.15 (2019), pp. 5329–5340. DOI: 10.1177/0954406219843568.

[10] José Carlos Ortiz Hernández and David I. Rosas Almeida. “Kinematic control in a four-wheeled Mecanum mobile robot for trajectory tracking”. In: *The Journal of Engineering* 2024.9 (2024), e70006. DOI: https://doi.org/10.1049/tje2.70006.

[11] Muhammad Umair Shafiq et al. “Real-time navigation of mecanum wheel-based mobile robot in a dynamic environment”. In: *Heliyon* 10.5 (2024), e26829. ISSN: 2405-8440. DOI: https://doi.org/10.1016/j.heliyon.2024.e26829.

[12] Luís Sarmento et al. “Remote control system for a mobile platform with four Mecanum wheels”. In: 2017. URL: https://api.semanticscholar.org/CorpusID:115672886.

[13] Wenkang Ji et al. “Application of Model Predictive Control to Trajectory Tracking of Mecanum Wheels”. In: *2022 IEEE 2nd International Conference on Electronic Technology, Communication and Information (ICETCI)*. 2022, pp. 45–49. DOI: 10.1109/ICETCI55101.2022.9832159.

[14] Veer Alakshendra and Shital Chiddarwar. “Adaptive robust control of Mecanum-wheeled mobile robot with uncertainties”. In: *Nonlinear Dynamics* 87 (Mar. 2017). DOI: 10.1007/s11071-016-3179-1.

[15] Anh Duc Pham and Hyeong-Joon Ahn. “Evaluation of Input Shaping Methods for the Nonlinear Vibration System Using a Furuta Pendulum”. In: *Journal of the Korean Society for Precision Engineering* 37 (Nov. 2020), pp. 827–833. DOI: 10.7736/JKSPE.020.056.

[16] Dongliang Wang et al. “Sliding mode observer-based model predictive tracking control for Mecanum-wheeled mobile robot”. In: *ISA Transactions* 151 (2024), pp. 51–61. ISSN: 0019-0578. DOI: https://doi.org/10.1016/j.isatra.2024.05.050.

[17] Madhu Sudan Das, Usha Rani Gogoi, and Sanjoy Mandal. “Hybrid Adaptive Sliding Mode Controller for Path Tracking of Wheeled Mobile Robot in Uncertainty”. In: *Ain Shams Engineering Journal* 16.12 (2025), p. 103640. ISSN: 2090-4479. DOI: https://doi.org/10.1016/j.asej.2025.103640.

[18] Ang Oon Thay et al. “Sliding Mode Controller for Trajectory Tracking Control of Autonomous Mobile Robot”. In: 2018. URL: https://api.semanticscholar.org/CorpusID:66982820.

[19] Roger Miranda Colorado, Jesus Rodriguez, and Luis Aguilar. *Observer-based Finite-Time Control of Perturbed Wheeled Mobile Robots*. Sept. 2023. DOI: 10.36227/techrxiv.24130800.

[20] Mehran Derakhshannia and Seyyed Sajjad Moosapour. “Disturbance observer-based sliding mode control for consensus tracking of chaotic nonlinear multi-agent systems”. In: *Mathematics and Computers in Simulation* 194 (2022), pp. 610–628. ISSN: 0378-4754. DOI: https://doi.org/10.1016/j.matcom.2021.12.017.

[21] Chen Zhang, Chen Cen, and Jiahui Huang. “An Overview of Model-Free Adaptive Control for the Wheeled Mobile Robot”. In: *World Electric Vehicle Journal* 15.9 (2024). ISSN: 2032-6653. DOI: 10.3390/wevj15090396.

[22] Pham Anh Tuan and Nguyen Manh Linh. “Trajectory Tracking Control of Omnidirectional Mobile Robots: a Model-Free Control-based Apprroach”. In: *Journal of Applied Science and Engineering* 27 (12 Mar. 2024), pp. 3687–3696. ISSN: 1560-6686. DOI: 10.6180/jase.202412_27(12).0009.

[23] Michel Fliess and Cédric Join. “Model-free control”. In: *International Journal of Control* 86 (May 2013). DOI: 10.1080/00207179.2013.810345.

[24] Jiahui Huang, Hua Chen, and Chao Shen. “Event-Triggered Model-Free Adaptive Control for Wheeled Mobile Robot with Time Delay and External Disturbance Based On Discrete-Time Extended State Observer”. In: *Journal of Dynamic Systems, Measurement and Control* 146 (Nov. 2023), pp. 1–14. DOI: 10.1115/1.4063996.

[25] Jacob Riera et al. “Sliding Mode Control for Trajectory Tracking of a TurtleBot3 Mobile Robot in Obstacle Environments”. In: *Engineering Proceedings* 77.1 (2024). ISSN: 2673-4591. DOI: 10.3390/engproc2024077007.

[26] Ching-Chih Tsai and Hsiao-Lang Wu. “Nonsingular terminal sliding control using fuzzy wavelet networks for Mecanum wheeled omnidirectional vehicles”. In: *International Conference on Fuzzy Systems*. 2010, pp. 1–6. DOI: 10.1109/FUZZY.2010.5584223.

[27] Hsu-Chih Huang and Shao-Kang Lin. “A Hybrid Metaheuristic Embedded System for Intelligent Vehicles Using Hypermutated Firefly Algorithm Optimized Radial Basis Function Neural Network”. In: *IEEE Transactions on Industrial Informatics* 15.2 (2019), pp. 1062–1069. DOI: 10.1109/TII.2018.2796556.

[28] Ronglin Ma et al. “New Adaptive Super-Twisting Extended-State Observer-Based Sliding Mode Scheme with Application to FOWT Pitch Control”. In: *Journal of Marine Science and Engineering* 12.6 (2024). ISSN: 2077-1312. DOI: 10.3390/jmse12060902. URL: https://www.mdpi.com/2077-1312/12/6/902.

[29] Yi Li et al. “A Super-Twisting Extended State Observer for Nonlinear Systems”. In: *Mathematics* 10.19 (2022). ISSN: 2227-7390. DOI: 10.3390/math10193584.

[30] Manh Nguyen et al. “Ballance Control of Ballbot - A Super-Twisting Extended Observer-Based Hierarchical Sliding Mode Control Approach”. In: Nov. 2025, pp. 620–629. ISBN: 978-981-95-1745-9. DOI: 10.1007/978-981-95-1746-6_69.

[31] İlyas Eker. "Sliding mode control with PID sliding surface and experimental application to an electromechanical plant". In: *ISA Transactions* 45.1 (2006), pp. 109–118. ISSN: 0019-0578. DOI: https://doi.org/10.1016/S0019-0578(07)60070-6.

[32] Thanh Pham and Chi-Ngon Nguyen. "Adaptive PID sliding mode control based on new Quasi-sliding mode and radial basis function neural network for Omni-directional mobile robot". In: *AIMS Electronics and Electrical Engineering* 7 (Mar. 2023), pp. 121–134. DOI: 10.3934/electreng.2023007.

[33] Kirtiman Singh. "Design of Sliding Mode PID Controller with Improved reaching laws for Nonlinear Systems". PhD thesis. Aug. 2014. DOI: 10.13140/RG.2.2.15462.42561.

[34] Kirtiman Singh and Prabin Padhy. *Modified PSO based PID Sliding Mode Control using Improved Reaching Law for Nonlinear systems*. Sept. 2022. DOI: 10.48550/arXiv.2209.09170.

[35] Mateo Vasquez et al. "A hybrid sliding mode control based on a nonlinear PID surface for nonlinear chemical processes". In: *Engineering Science and Technology an International Journal* 40 (Apr. 2023). DOI: 10.1016/j.jestch.2023.101361.